

Semi-vortex solitons and their excited states in spin-orbit-coupled binary bosonic condensates

Haiming Deng^{1,2,5}, Jinqing Li^{1,2,5}, Zhaopin Chen³, Yaohui Liu⁵, Dong Liu⁵, Chunzhi Jiang^{1,2,5}, Chao Kong^{1,2,5a}, and Boris A. Malomed⁴

¹ School of Physics and Electronic-Electrical Engineering, Xiangnan University, Chenzhou 423000, China

² Microelectronics and Optoelectronics Technology Key Laboratory of Hunan Higher Education, Xiangnan University, Chenzhou 423000, China

³ Physics Department and Solid-State Institute, Technion, Haifa 32000, Israel

⁴ Instituto de Alta Investigación, Universidad de Tarapacá, Casilla 7D, Arica, Chile ^b

⁵ Hunan Engineering Research Center of Advanced Embedded Computing and Intelligent Medical Systems, Xiangnan University, Chenzhou 423000, China

It is known that two-dimensional two-component fundamental solitons of the *semi-vortex* (SV) type, with vorticities $(s_+, s_-) = (0, 1)$ in their components, are stable ground states (GSs) in the spin-orbit-coupled (SOC) binary Bose-Einstein condensate with the contact self-attraction acting in both components, in spite of the possibility of the critical collapse in the system. However, excited states (ESs) of the SV solitons, with the vorticity set $(s_+, s_-) = (S_+, S_+ + 1)$ and $S_+ = 1, 2, 3, \dots$, are unstable in the same system. We construct ESs of SV solitons in the SOC system with opposite signs of the self-interaction in the two components. The main finding is *stability* of the ES-SV solitons, with the extra vorticity (at least) up to $S_+ = 6$. The threshold value of the norm for the onset of the critical collapse, N_{thr} , in these excited states is *higher* than the commonly known critical value, $N_c \approx 5.85$, associated with the single-component Townes solitons, N_{thr} increasing with the growth of S_+ . A velocity interval for stable motion of the GS-SV solitons is found too. The results suggest a solution for the challenging problem of the creation of stable vortex solitons with high topological charges.

Keywords: Bose-Einstein condensate; Spin-orbit coupling; Semi-vortex solitons; Soliton dynamics

I. INTRODUCTION

The experimental creation of Bose-Einstein condensates (BECs) in ultracold atomic gases [1–3] provides an ideal platform for exploring various states in quantum superfluids, such as vortices [4, 5], stable dark [6, 7] and bright [8–10] one-dimensional (1D) solitons, weakly unstable (therefore, observable) 2D solitons of the Townes type [11, 12], stable quantum droplets in the 2D [13, 14] and 3D [15], and other dynamical modes [16–20]. The cubic self-attractive (mean-field) nonlinearity readily predicts solitons in the 2D and 3D free space, but these solitons are rendered completely unstable by the critical (2D) and supercritical (3D) collapse which takes place in the same settings [22–26] (unless the effect of the quantum fluctuations manifests itself, providing the collapse-suppressing quartic self-interaction [27–29], which stabilizes the quantum droplets [13–15]). The instability gives rise to the challenging problem of the prediction and creation of *stable* 2D and 3D matter-wave solitons, including those with embedded vorticity, that may be maintained by the mean-field nonlinear interactions in appropriately modified physical settings [26].

Various methods have been proposed to achieve this purpose. On the one hand, it has been predicted that long-range interactions in BEC of dipole atoms, carrying permanent magnetic moments, can support stable 2D or even 3D matter-wave solitons [30–34]. Another possibility is to use the combination of the spin-orbit coupling (SOC) between two components of binary BEC and attractive mean-field nonlinearity [35–42]. However, the stabilization provided by these systems is limited to the fundamental (ground state, GS) solitons. In particular, the SOC system makes it possible to find 2D excited-state (ES) solitons, which, however, are completely unstable [35]. Naturally, ES solitons exhibit a richer amplitude and phase structure than their GS counterparts, which makes stabilization of ES solitons another relevant problem, that has not been resolved in previous works [26, 43].

The objective of this work is to predict *stable* 2D solitons, *including* ones of the ES type, in the spin-orbit-coupled binary BEC with opposite signs (attraction and repulsion) of the self-interactions in the two components. This arrangement, which was not addressed previously, may be realized in the experiment by means of the Feshbach-resonance technique, applied to the two-component BEC [44–47]. The analysis produces solitons of the semi-vortex (SV) type, defined as in Ref. [35]: these are GSs with the vorticity set $(s_+, s_-) = (0, 1)$ of their two components, and ESs with extra vorticity $S_+ = 1, 2, 3, \dots$ added to each component, i.e., with the set

$$\{s_+, s_-\} = \{S_+, S_+ + 1\}. \quad (1)$$

^a Corresponding Author: superkong@xnu.edu.cn

^b Sabbatical address

Our analysis demonstrates that the ES solitons may be stable, at least, up to $S_+ = 6$. Systematically collected numerical results reveal that the ES solitons with the vorticity in both components exist provided that their total does not exceed a collapse threshold N_{thr} , which surpasses the well-known threshold ($N_c \approx 5.85$) for the fundamental (Townes) single-component solitons in the free 2D space [21, 22]. The value N_{thr} increases with the growth of the additional vorticity S_+ . These findings offer, for the first time, a solution of the problem of the creation of stable ES solitons in SOC systems.

The following presentation is structured as follows. In Section 2, we introduce the model, based on a system of two spin-orbit-coupled Gross-Pitaevskii equations (GPEs), with the opposite signs of the cubic nonlinearity in the two components. In Section 3, we produce SV soliton solutions of the GS and ES types and test their stability by means of numerical methods. In Section 4, we address moving SV solitons and their stability, which is a nontrivial problem, as the SOC breaks the system's Galilean invariance. A critical velocity V_{cr} , up to which the stable moving solitons exist, is identified as a function of the total norm N . Finally, Section 5 concludes the paper.

II. THE MODEL

In its scaled form, the 2D system of coupled GPEs for the spinor wave function, $\Psi = \{\Psi_+, \Psi_-\}$, with the SOC of the Rashba type, is written as

$$\begin{aligned} i\frac{\partial\Psi_+}{\partial t} &= -\frac{1}{2}\nabla^2\Psi_+ + \left(\frac{\partial}{\partial x} - i\frac{\partial}{\partial y}\right)\Psi_- \\ &\quad - (g_+|\Psi_+|^2 + \gamma|\Psi_-|^2)\Psi_+, \\ i\frac{\partial\Psi_-}{\partial t} &= -\frac{1}{2}\nabla^2\Psi_- - \left(\frac{\partial}{\partial x} + i\frac{\partial}{\partial y}\right)\Psi_+ \\ &\quad - (-g_-|\Psi_-|^2 + \gamma|\Psi_+|^2)\Psi_-, \end{aligned} \tag{2}$$

where positive g_+ and g_- coefficients are strengths of the self-attraction and repulsion in the components Ψ_+ and Ψ_- , respectively, and γ is the cross-interaction strength. The linearized form of Eqs. (2) and (3) for plane-wave solutions, $\Psi_{\pm} \sim \exp(-i\mu_{\text{linear}}t + ik_x x + ik_y y)$, yields the dispersion relation

$$\mu_{\text{linear}} = \pm k + k^2/2, \tag{4}$$

where $k^2 = k_x^2 + k_y^2$. An obvious corollary of Eq. (4) is that solitons may exist in the semi-infinite bandgap,

$$\mu < \mu_{\text{cutoff}} = -1/2, \tag{5}$$

in which expression (4) cannot take its value while the wavenumber varies in the region of $0 \leq k < \infty$.

Solutions to Eqs. (2) and (3) for solitons of the SV type, with a real chemical potential $\mu < 0$ and the set of vorticities (1) in its components, can be looked for as (cf. Ref. [35])

$$\begin{aligned} \Psi_+ &= \exp(-i\mu t + iS_+\theta) r^{S_+} \Phi_+(r^2), \\ \Psi_- &= \exp(-i\mu t + i(1+S_+)\theta) r^{1+S_+} \Phi_-(r^2). \end{aligned} \tag{6}$$

The substitution of ansatz (6) in Eqs. (2) and (3) leads to system of ordinary differential equations for real functions $\Phi_{\pm}(r^2)$, cf. Ref. [35]:

$$\begin{aligned} \mu\Phi_+ &= -2[r^2\Phi_+'' + (1+S_+)\Phi_+'] \\ &\quad + 2[r^2\Phi_-' + (1+S_+)\Phi_-] \\ &\quad - [g_+(r^2)^{S_+}\Phi_+^2 + \gamma(r^2)^{1+S_+}\Phi_-^2]\Phi_+, \end{aligned} \tag{7}$$

$$\begin{aligned} \mu\Phi_- &= -2[r^2\Phi_-'' + (2+S_+)\Phi_-'] - 2\Phi_+ \\ &\quad - [-g_-(r^2)^{1+S_+}\Phi_-^2 + \gamma(r^2)^{S_+}\Phi_+^2]\Phi_-, \end{aligned} \tag{8}$$

where $\Phi'_{\pm} \equiv d\Phi_{\pm}/d(r^2)$.

To establish a relationship between the size and structure of the SV soliton and the magnitude of the cross- and self-interaction strengths, we define the effective radius of the soliton and the norm ratio of the two components, respectively, as follows:

$$R = \left(\frac{\int r^2 n(\mathbf{r}) d\mathbf{r}}{\int n(\mathbf{r}) d\mathbf{r}} \right)^{1/2}, \quad F = \frac{N_-}{N_+}, \quad (9)$$

where $n(r) = |\Psi_+(r)|^2 + |\Psi_-(r)|^2$ is the total density of the solution, the total and component norms being

$$N = \int n(\mathbf{r}) d\mathbf{r} \equiv N_+ + N_-. \quad (10)$$

Obviously, N is a dynamical invariant of the system of Eqs. (2) and (3). In the analysis following below, we treat (N, g_+, g_-, γ) as a set of the system's control parameters.

The system also conserves the energy (Hamiltonian),

$$\begin{aligned} E = & \int \left[\frac{1}{2} (|\nabla \Psi_+|^2 + |\nabla \Psi_-|^2) \right. \\ & + \Psi_+^* \left(\frac{\partial}{\partial x} - i \frac{\partial}{\partial y} \right) \Psi_- + \Psi_+ \left(\frac{\partial}{\partial x} + i \frac{\partial}{\partial y} \right) \Psi_-^* \\ & \left. - \frac{g_+}{2} |\Psi_+|^4 + \frac{g_-}{2} |\Psi_-|^4 - \gamma |\Psi_+|^2 |\Psi_-|^2 \right] d\mathbf{r}, \end{aligned} \quad (11)$$

with $*$ standing for the complex conjugate. It is relevant to mention that, in terms of the polar coordinates (r, θ) and spinor wave function defined as $\{\tilde{\Psi}_+ \equiv e^{i\theta} \Psi, \Psi_-\}$, the Hamiltonian (11) is written as

$$\begin{aligned} E = & \int_0^\infty r dr \int_0^{2\pi} d\theta \left[\frac{1}{2} (|\nabla \Psi_+|^2 + |\nabla \Psi_-|^2) \right. \\ & + \tilde{\Psi}_+^* \left(\frac{\partial}{\partial r} - \frac{i}{r} \frac{\partial}{\partial \theta} \right) \Psi_- + \tilde{\Psi}_+ \left(\frac{\partial}{\partial r} + \frac{i}{r} \frac{\partial}{\partial \theta} \right) \Psi_-^* \\ & \left. - \frac{g_+}{2} |\Psi_+|^4 + \frac{g_-}{2} |\Psi_-|^4 - \gamma |\Psi_+|^2 |\Psi_-|^2 \right]. \end{aligned} \quad (12)$$

According to the Noether theorem [52], the invariance of expression (12) with respect to an arbitrary rotation, $\theta \rightarrow \theta + \Delta\theta$, implies that the angular momentum,

$$\begin{aligned} M = & -i \int_0^\infty r dr \int_0^{2\pi} d\theta \left(\tilde{\Psi}_+^* \frac{\partial}{\partial \theta} \tilde{\Psi}_+ + \Psi_-^* \frac{\partial}{\partial \theta} \Psi_- \right) \\ \equiv & \int_0^\infty r dr \int_0^{2\pi} d\theta \left[-i \left(\Psi_+^* \frac{\partial}{\partial \theta} \Psi_+ + \Psi_-^* \frac{\partial}{\partial \theta} \Psi_- \right) + |\Psi_+|^2 \right], \end{aligned} \quad (13)$$

is also a dynamical invariant. Note that the substitution of ansatz (6) in expression (13) yields a simple relation between the angular momentum and norm (10) of the stationary states, which applies equally well to the GS and ESs:

$$M = (1 + S_+) N. \quad (14)$$

III. GROUND AND EXCITED STATES OF SEMI-VORTEX SOLITONS

Following Refs. [50, 51], SV solitons can be produced in the numerical form by means of the imaginary-time integration method [53], applied to Eqs. (2) and (3) with an input which follows the structure of ansatz (6),

$$\begin{aligned} \Psi_+(t=0) &= A_+ r^{S_+} \exp(-\alpha_+ r^2 + i S_+ \theta), \\ \Psi_-(t=0) &= A_- r^{1+S_+} \exp(-\alpha_- r^2 + i(1+S_+) \theta), \end{aligned} \quad (15)$$

where A_\pm and α_\pm are positive real constants. As said above, the SVs of the GS and ES types correspond, respectively, to $S_+ = 0$ and $S_+ = 1, 2, 3, \dots$, respectively. The stability of the solitons was then identified with the help of systematic real-time simulations of their perturbed evolution in the framework of Eqs. (2) and (3).

A. Ground-state (GS) solitons

A typical example of a stable solution which represents the GS of the SV type, with norm $N = 4$ and parameters $g_+ = g_- = \gamma = 1$ in Eqs. (2) and (3), is displayed in Fig. 1, where the densities, $|\Psi_{\pm}|^2$, demonstrate perfect axisymmetric patterns. Parameters (9) for this solution are $R = 1.2377$ and $F = 0.5667$.

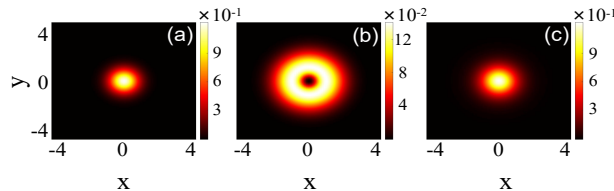


FIG. 1. An example of a stable GS soliton, corresponding to ansatz (6) with $S_+ = 0$, with the total norm $N = 4$ (see Eq. (10)), produced by the numerical solution of Eqs. (2) and (3) with $g_{\pm} = \gamma = 1$. Panels (a), (b) and (c) display, severally, the density patterns of the zero-vorticity and vortex components, $|\Psi_+|^2$ and $|\Psi_-|^2$, and the total density, $|\Psi_+|^2 + |\Psi_-|^2$.

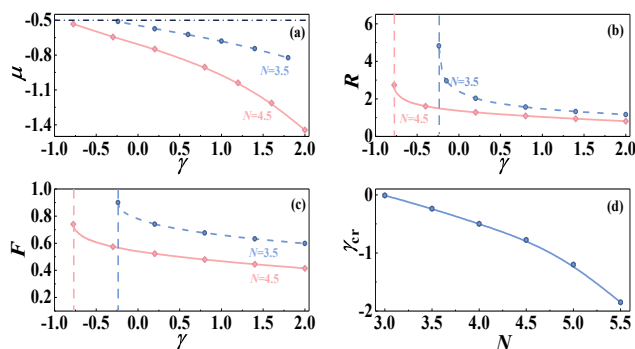


FIG. 2. Panels (a), (b), and (c) show, respectively, the chemical potential, effective radius R , and the component-norm ratio F (see Eq. (9)) of the ground-state SV solitons vs. the cross-interaction strength γ for fixed values of the total norm, $N = 3.5$ and 4.5 (the blue dashed and red solid curves, respectively). In panel (a), the cutoff value $\mu = -1/2$, which is the boundary of the semi-infinite bandgap (see Eq. (5)), marked by the horizontal dashed-dotted line. The respective critical values γ_{cr} of the cross-interaction strength, at which the cutoff is attained, $\mu(\gamma = \gamma_{\text{cr}}) = -1/2$, are marked by the vertical dashed lines panels (b) and (c). Further, γ_{cr} is plotted as a function of the norm in panel (d). In this setting, we fix $g_{\pm} = 1$ in Eqs. (2) and (3).

For two typical values of the total norm, $N = 4.5$ and $N = 3.5$, properties of the GS solutions are summarized in Figs. 2(a,b,c), where the chemical potential, effective radius, and the norm ratio of the two components, defined as per Eq. (9), are plotted vs. the cross-interaction strength γ in Eqs. (2) and (3). In these plots, γ takes both positive and negative values, which correspond, respectively, to the cross-attraction and repulsion, while the self-interaction coefficients are fixed as $g_+ = g_- = 1$. In Fig. 2(a), the SV soliton suffers delocalization, turning into an infinitely broad state with an infinitely small amplitude, as chemical potential μ is reaching the limit value (5), $\mu_{\text{cutoff}} = -1/2$, at $\gamma \rightarrow \gamma_{\text{cr}}(N = 4.5) = -0.775$ or $\gamma_{\text{cr}}(N = 3.5) = -0.24$. For other values of the norm (in the interval of $3 < N < 5.5$), the dependence of γ_{cr} on N is plotted in Fig. 2(d). Self-trapped bound states (solitons) do not exist if γ is “too negative”, taking values $\gamma < \gamma_{\text{cr}}(N)$, as the self-trapping is obviously impossible when the overall nonlinearity is self-repulsive. The transition to the delocalization is also demonstrated by the increase of the effective size R (defined as per Eq. (9)) as γ is approaching γ_{cr} .

The norm ratio F of the vortical and zero-vorticity components (see Eq. (9)) takes values $F < 1$ because, naturally, the central hole in the former component makes its norm smaller, cf. Figs. 1(b) and (a). The fact that the larger part of the norm is concentrated in the self-attractive components, Ψ_+ , helps to minimize the solitons’ energy and thus stabilize them. It may also be possible to construct SV solitons with a *reverse structure*, i.e., the zero-vorticity and vortical components carried by wave functions Ψ_- and Ψ_+ , respectively (their ES counterparts can be introduced too). In fact, it is easier to construct such reverse-structured SV solitons as solutions (6) with $S_+ \geq 0$ (as adopted above), but for opposite signs of the nonlinearity coefficients, *viz.*, $g_+ < 0$ and $g_- < 0$ in Eqs. (2) and (3). While we did not analyze such reverse SV solutions in detail, it is implausible that they may be stable, as they place a larger share of the norm, corresponding to the zero-vorticity component, under the action of the self-repulsion, which makes the total energy larger, leading to destabilization. Thus, while both the GS and ES species of the SV solitons keep

the axial isotropy of the solutions. as is obvious from Eqs. (6) and (15), the solutions break the chiral symmetry, as they favor only positive values of the angular momentum, according to Eq. (14).

B. Excited-state (ES) solitons

Stable higher-order (ES) soliton solutions have been constructed by applying the imaginary-time-simulation method to Eqs. (2) and (3) with the input taken as per Eq. (15), up to S_+ (still higher values of S_+ were not considered here, cf. Refs. [50, 51]). Typical examples of the so density and phase structure of the so constructed stable ES solitons with $S_+ = 1, 2, 3$ and 4 are displayed in Fig. 3, where we set $g_{\pm} = \gamma = 1$ and $N = 4$.

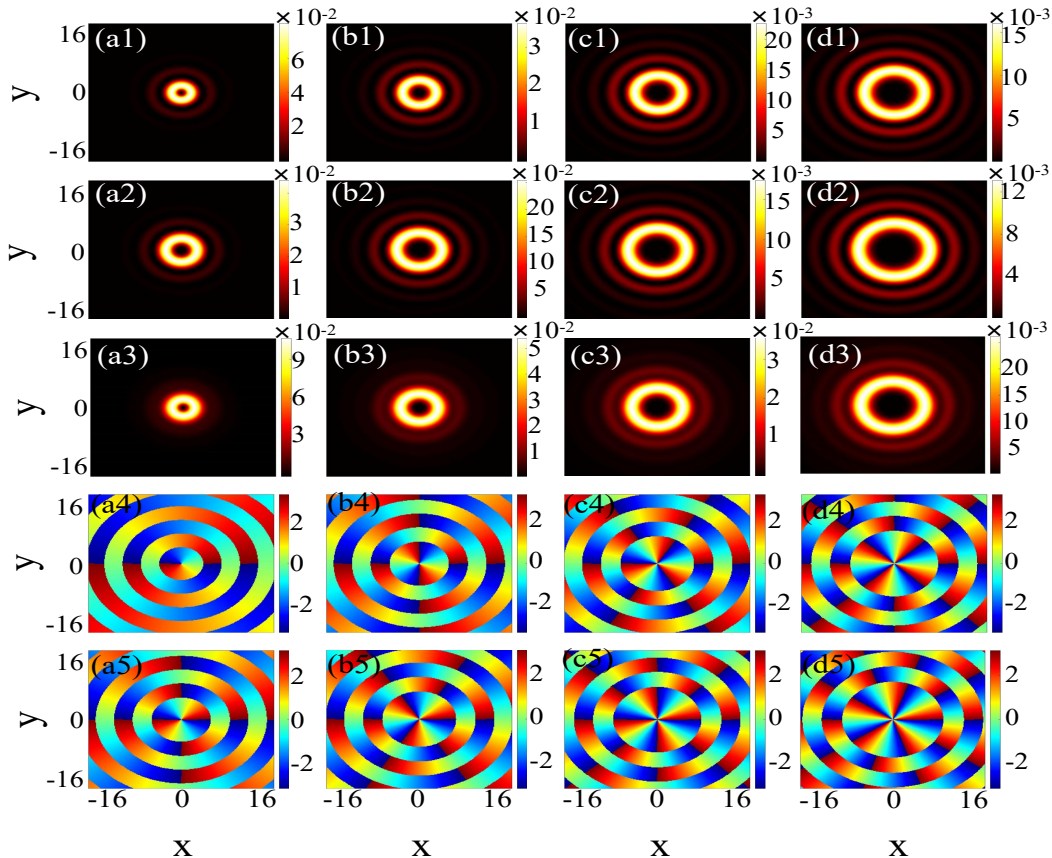


FIG. 3. The first and second rows: density patterns of the Ψ_+ and Ψ_- components of the ES-SV solitons. The third row: the total-density patterns, $|\Psi_+|^2 + |\Psi_-|^2$, for the same states. The fourth and fifth rows: phase patterns of the components Ψ_+ and Ψ_- , respectively. From left to right: $S_+ = 1, 2, 3$ and 4. Here, the parameters are fixed as $g_{\pm} = \gamma = 1$ and $N = 4$.

The systematic numerical analysis has identified the stability charts for the ES-SV solitons in the parameter plane of (N, γ) , which are presented in Figs. 4(a)-(d) for $S_+ = 1, 2, 3$, and 4 (in fact, stable ES solitons have been found up to $S_+ = 6$, and may plausibly exist for still larger values of S_+). The ESs are stable and unstable in the blue and red areas, respectively. The stable ES solitons exist with the total norm taking values below the collapse threshold N_{thr} , which surpasses the well-known collapse threshold ($N_c \approx 5.85$) for the single-component fundamental Townes solitons in free 2D space [22], as well as for the GS-SV solitons [35]. As the boundaries between stable and collapsing ES solitons, the threshold values for the onset of the critical 2D collapse are $N_{\text{thr}} = 6.6, 8.5, 9.6$, and 14 for $S_+ = 1, 2, 3$ and 4, respectively. Thus, the collapse-free area expands with the increase of the extra topological charges, S_+ , or, in other words, with the increase of the soliton's angular momentum, pursuant to Eq. (14). The corresponding relative expansion of the area is $(N_{\text{thr}} - N_c)/N_c = 12.8\%, 45.3\%, 64.1\%$ and 139% for $S_+ = 1, 2, 3$ and 4, respectively.

As said above, the stability of the ES-SV solitons was verified through systematic real-time simulations of their perturbed evolution, using the split-step fast-Fourier-transform algorithm. Typical examples of the stable evolution of the solitons with $S_+ = 1, 2, 3$, and 4 are displayed in Figs. 5(a1-a4), respectively. In these plots, parameter values (N, γ) are chosen from the stability region delineated in Fig. 4. On the other hand, when parameters (N, γ) are taken

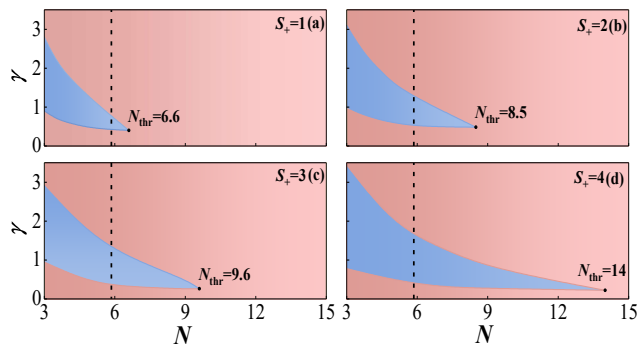


FIG. 4. The ES-SV solitons are stable/unstable in the blue/red areas of the parameter plane of (N, γ) for the extra topological charges $S_+ = 1$ (a), $S_+ = 2$ (b), $S_+ = 3$ (c), and $S_+ = 4$ (d). Other parameters are fixed as $g_{\pm} = 1$.

in instability areas of Fig. 4, the simulations demonstrate spontaneous destruction of the SV solitons in the course of the long-time propagation in Figs. 5(b1-b4).

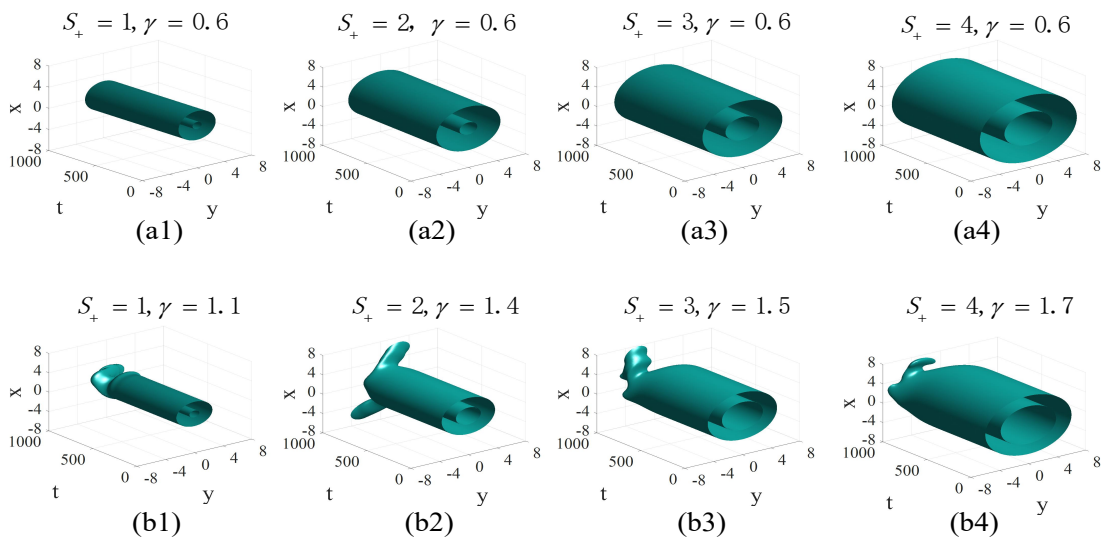


FIG. 5. The stable simulated long-real-time evolution of stable ES-SV is displayed by means of density patterns of $|\Psi_+|^2$, for $(S_+, \gamma) = (1, 0.6)$ (a1), $(2, 0.6)$ (a2), $(3, 0.6)$ (a3) and $(4, 0.6)$ (a4). Examples of the unstable evolution are presented in panels (b1-b4) for $(S_+, \gamma) = (1, 1.1)$ (b1), $(2, 1.4)$ (b2), $(3, 1.5)$ (b3) and $(4, 1.7)$ (b4). Here, fixed parameters are $g_{\pm} = 1$ and $N = 6$.

To explain the counter-intuitive phenomenon observed in Fig. 4, where the stability area of the ES-SV solitons expands with then increase of the extra topological charge S_+ , the corresponding ratio $F = N_-/N_+$ (see Eq. (9)) is displayed in Fig. 6(a) vs. S_+ for fixed parameters $(N, g_{\pm}, \gamma) = (4, 1, 1)$. The growing dependence $F(S_+)$ implies the transfer of the condensate into the self-repulsive component Ψ_- , which naturally inhibits the onset of the collapse.

To further quantify properties of the ES-SV solitons, we fix parameters $(N, g_-, \gamma) = (4, 1, 1)$ and vary strength g_+ of the self-attraction component in component Ψ_- , plotting the respective dependences $\mu(g_+)$ for different values of S_+ in Fig. 6(b). An essential observation is that $\mu(g_+)$ curves satisfy the Vakhitov-Kolokolov (VK) criterion, $d\mu/dg_+ < 0$, which is a well-known necessary stability condition for solitons maintained by a self-attractive nonlinearity [24, 48] (the VK criterion takes this form for the fixed norm, while the strength of the self-attraction varies).

Next, Fig. 7 displays the dependence of μ and effective soliton's radius R (see Eq. (9)) as functions of the self-repulsion strength g_- in component Ψ_- for different values of S_+ , fixing other parameters as $(N, g_+, \gamma) = (4, 1, 1)$. In particular, positive slope, $d\mu/dg_- > 0$ of the $\mu(g_-)$ curves in Fig. 7(a) implies that the ES-SV families satisfy the *anti-VK criterion*, which is a necessary stability condition for solitons with respect to the variation of the *self-repulsion strength* [49]. In Fig. 7(b), the growth of the soliton's radius $R(g_-)$ with the increasing of g_- demonstrates a natural trend to expansion of the bound state under the action of stronger self-repulsion.

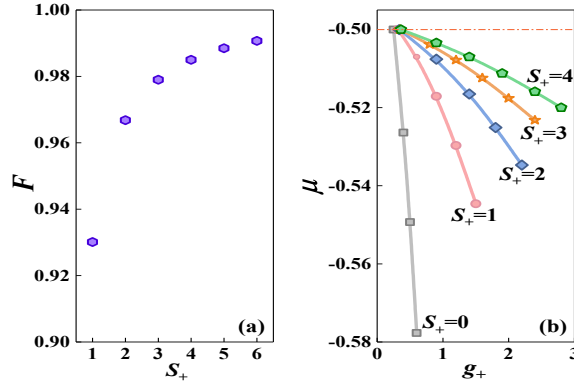


FIG. 6. (a) Ratio $F = N_-/N_+$ (see Eq. (9)) for the ES-SV solitons vs. the additional; topological charge S_+ , with fixed parameters $(N, g_+, \gamma) = (4, 1, 1)$. (b) The solitons' chemical potential μ , for different values of S_+ , as a function of the self-interaction strength g_+ in component Ψ_+ , with fixed parameters $(N, g_-, \gamma) = (4, 1, 1)$.

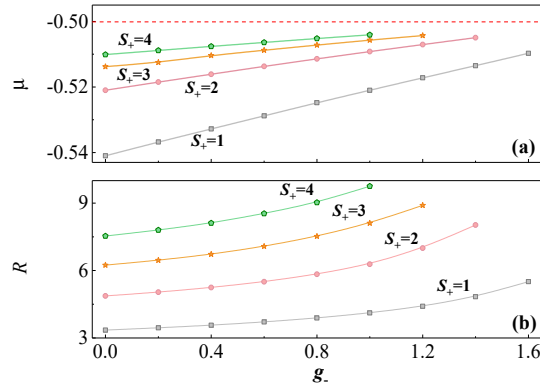


FIG. 7. (a,b) Chemical potential μ and effective radius R of the ES-SV solitons vs. the self-repulsion strength g_- in component Ψ_- for different values of the additional topological charge S_+ , with fixed parameters $(N, g_+, \gamma) = (4, 1, 1)$.

IV. STABILITY OF MOVING 2D SOLITONS

The SO coupling breaks the Galilean invariance of GPEs, hence mobility of SOC-affected solitons is a nontrivial problem. It was reported [35] that, in the case of $g_- = -g_+ \equiv 1$ and $\gamma < 1$ (equal strengths of the self-attraction in both components of Eqs. (2) and (3), exceeding the strength of the inter-component attraction), SVs can move stably, but only in a narrow interval of velocities along the y axis, e.g., $|V_y| \leq V_{cr} \approx 0.03$ for the norm $N = 3.7$. A much larger stability interval, e.g., $|V_y| \leq V_{cr}^{(MM)} \approx 1.8$ for $N = 3.1$ and $\gamma = 2$, was found for moving *mixed-mode (MM) solitons*, which are stable in the case of $\gamma > 1$, when the SV solitons are completely unstable. The name of the MM states implies that they are generated by inputs which feature mixtures of terms with vorticities $\{0, -1\}$ in component Ψ_+ , and $\{0, +1\}$ in Ψ_- . Actually, solutions for GS solitons moving with velocity $V > V_{cr}$ converge to MM states instead of the SV ones [35].

The current system produces stably moving SV solitons in much broader velocity interval. To analyze this issue, it is natural to apply the formal Galilean boost, with the velocity vector (V_x, V_y) , to Eqs. (2) and (3), which would keep the equations invariant in the absence of the SOC term:

$$\begin{aligned}
 i \frac{\partial \tilde{\Psi}_+}{\partial t} &= -\frac{1}{2} \nabla_+^2 \tilde{\Psi} + \left(\frac{\partial}{\partial \tilde{x}} - i \frac{\partial}{\partial \tilde{y}} \right) \tilde{\Psi}_- \\
 -(g_+ |\tilde{\Psi}_+|^2 + \gamma |\tilde{\Psi}_-|^2) \tilde{\Psi}_+ + (iV_x + V_y) \tilde{\Psi}_-, &
 \end{aligned} \tag{16}$$

$$\begin{aligned}
 i \frac{\partial \tilde{\Psi}_-}{\partial t} &= -\frac{1}{2} \nabla_-^2 \tilde{\Psi} - \left(\frac{\partial}{\partial \tilde{x}} + i \frac{\partial}{\partial \tilde{y}} \right) \tilde{\Psi}_+ \\
 -(-g_- |\tilde{\Psi}_-|^2 + \gamma |\tilde{\Psi}_+|^2) \tilde{\Psi}_- + (-iV_x + V_y) \tilde{\Psi}_+, &
 \end{aligned} \tag{17}$$

where we define the transformed wave function and moving coordinates:

$$\tilde{\Psi}_{\pm} \equiv \exp\left(-\frac{i}{2}(V_x^2 + V_y^2)t + iV_x x + iV_y y\right) \Psi_{\pm}(\tilde{x}, \tilde{y}, t), \quad (18)$$

$$\tilde{x} \equiv x - V_x t, \quad \tilde{y} \equiv y - V_y t. \quad (19)$$

Solving the system of Eqs. (16) and (17) by means of the imaginary-time-integration method, we find that the moving GS-SV solitons remain stable in a velocity interval $V \leq V_{\text{cr}}$ which is much broader than in the system with $g_- = -g_+$, $\gamma = 0$, which was addressed in Ref. [35]. Due to the axial isotropy of the system's Hamiltonian, written in the form of Eq. (12), and the isotropic shape of the general ansatz (6) for the solutions, V_{cr} does not depend on the direction of the velocity vector.

Typical examples of the stable moving GS-SV solitons with velocity vectors $(V_x, V_y) = (0, 0.09)$, $(0.09, 0)$, and $(0.0636, 0.0636)$ are presented, severally, in the top, middle, and bottom rows of Fig. 8, for fixed parameters $(N, \gamma, g_{\pm}, S_+) = (4, 1, 1, 0)$. In this case, V_{cr} is very close to the velocity value 0.09 for which the solutions are produced in the top and middle rows of Fig. 8. The velocity corresponding to the bottom row, $V = \sqrt{2} \times 0.06 \approx 0.085$, is also close to this value.

These results are summarized in Fig. 9 by dependences of V_{cr} on parameters $g_+ = g_- \equiv g$ and N . In particular, Fig. 9(a) shows that, in the range of $3 \leq N \leq 5.5$, the critical velocity steeply increases with the growth of N . This dependence is explained by the fact that stronger nonlinearity, which corresponds to larger norm, makes the destabilizing effect of the velocity in Eqs. (16) and (17) effectively weaker. The same argument explains the growth of V_{cr} with the increase of g in Fig. 9(b). The availability of the stably moving SV solitons suggests considering collisions between them. In particular, we have performed simulations for the collisions between ones moving with opposite velocities $V_x = \pm 0.03$ in Fig. 10. Figs. 10(a)-10(c) display the contour plots of $|\Psi_+|^2 + |\Psi_-|^2$ at $t = 510$, $t = 1035$ and $t = 1500$, respectively. The arrows in the figures represent the direction of solitons motion. Isosurface plot is displayed in Fig. 10(d). Clearly, the solitons repel each other and maintain their shapes after the rebound, i.e., they collide elastically.

As concerns the ESs with $S_+ \geq 1$, a preliminary analysis demonstrate that the corresponding inputs converge to the ground state, as a result of the imaginary-time simulations of Eqs. (16) and (17). A systematic consideration of this problem should be a subject of a separate work. At $V > V_{\text{cr}}$ the imaginary-time solution of Eqs. (16) and (17) demonstrates that the same input, which produces the GS-SV solitons at $V < V_{\text{cr}}$, gives rise to stable solitons of the above-mentioned MM type, similar to what was found in Ref. [35]. The typical example of the mixed-mode solitons found at $V > V_{\text{cr}}$ is displayed in Fig. 11.

V. CONCLUSION

The objective of this work is to study 2D SV (semi-vortex) solitons in the binary BEC with two components coupled by the linear spin-orbit interaction and nonlinear inter-component attraction. Unlike the previous work [35], we consider the system of coupled GPEs (Gross-Pitaevskii equations) with the self-attraction and repulsion in the two components. The most essential finding is that, in contrast to Ref. [35], where the ES (excited-state) solitons, produced by the addition of the same vorticity S_+ to both components of the GS (ground-state) soliton of the SV type, are completely unstable in the case of the self-attraction acting in both components, the ES-SV solitons produced by the present system have their stability regions, expanding with the increase of S_+ (at least, up to $S_+ = 4$). In particular, the critical norm, at which the collapse sets in the GPE system, also increases with the growth of S_+ . The study of moving GS-SV solitons demonstrates that they exist in the interval of velocities, $0 < V < V_{\text{cr}}$, which is essentially larger than the one reported in Ref. [35]. The critical velocity, V_{cr} , steeply increases with the growth of the norm and nonlinearity strength. These findings suggest new directions for experimental studies of the nonlinear matter-wave dynamics in the SOC (spin-orbit-coupled) BEC, especially as concerns the challenging problem of creation of stable solitons with high embedded vorticity.

A natural direction for further research is to extend the current analysis for ESs of solitons of the MM (mixed-mode) type, which combine terms with vorticities 0 and ± 1 in the two components. It may be also interesting to explore Josephson oscillations between ESs of solitons of the SV and MM types, cf. Ref. [54]. A challenging possibility is to seek for (meta-) stable ESs of solitons in three-dimensional SOC BEC, cf. Ref. [40].

Recently, much interest in the experimental [13–15, 55, 56] and theoretical [29, 57–61] work was drawn to self-bound quantum droplets in BEC stabilized by effects of quantum fluctuations. In this connection, it will be relevant to construct stable ESs of spin-orbit-coupled quantum droplets of the SV and MM types. To this end, it is necessary to use SOC GPEs including the Lee-Huang-Yang corrections [59].

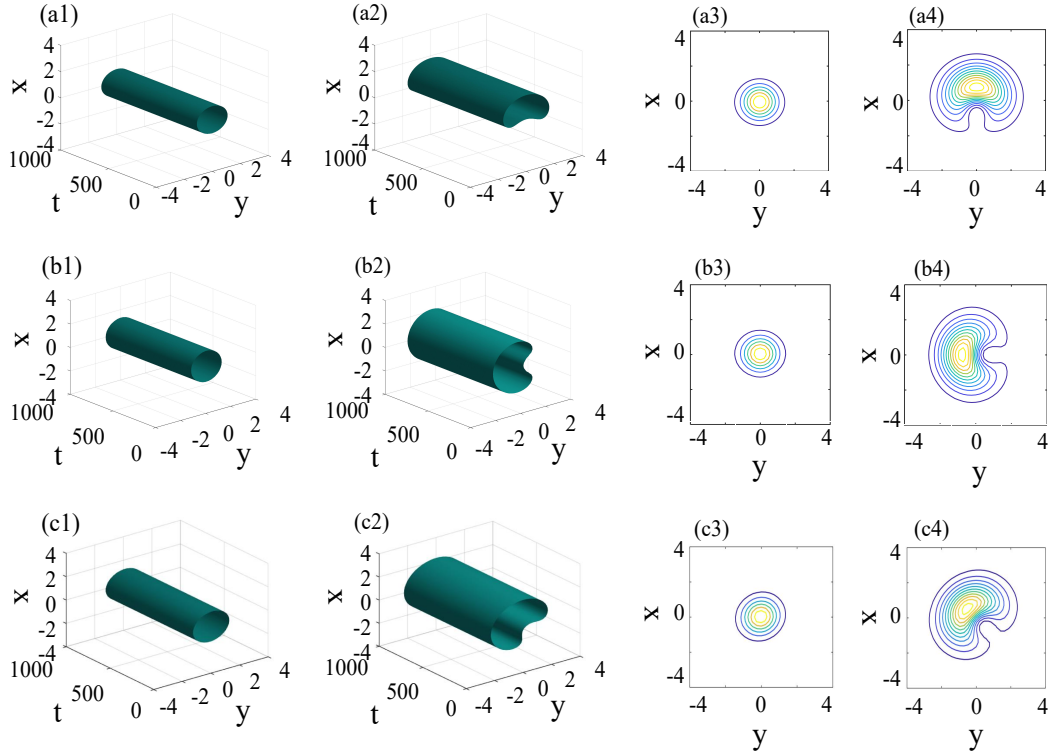


FIG. 8. Isosurface and contour plots of the component densities $|\Psi_+|^2$ and $|\Psi_-|^2$ (panels (a1), (b1), (c1); (a3), (b3), (c3), and (a2), (b2), (c2); (a4), (b4), (c4), respectively) for stable moving GS-SV solitons, with parameters $(N, g_{\pm}, \gamma, S_+) = (4, 1, 1, 0)$. Panels (a1)-(a4), (b1)-(b4), and (c1)-(c4) represent the solitons with velocities $(V_x, V_y) = (0, 0.09)$, $(V_x, V_y) = (0.09, 0)$, and $(V_x, V_y) = (0.0636, 0.0636)$, respectively.

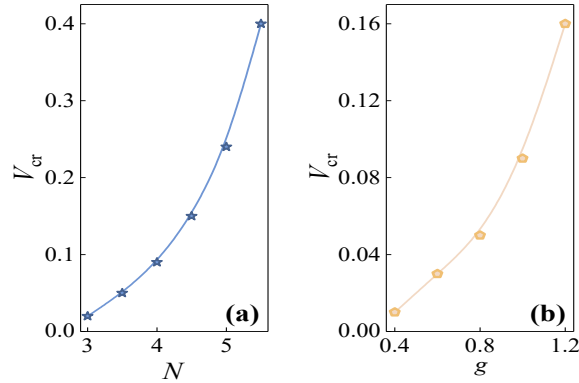


FIG. 9. (a) The critical velocity, V_{cr} , up to which stably moving GS-SV solitons are produced by the imaginary-time solution of Eqs. (16) and (17), vs. N for fixed parameters $(g_{\pm}, \gamma) = (1, 1)$. (b) V_{cr} vs. $g_+ = g_- \equiv g$ for fixed parameters $(N, \gamma) = (4, 1)$.

ACKNOWLEDGMENTS

The authors appreciate valuable discussions with Profs. Yongyao Li and Bin Liu (Foshan University). This work was supported by the Project of Hunan Provincial Education Office under Grant No. 23A0593, 23B0774, Scientific Research Foundation of Xiangnan University for High-Level Talents, the Applied Characteristic Disciplines of Electronic Science and Technology of Xiangnan University (XNXY20221210), Science and Technology Innovative Research Team in Higher Educational Institutions of Hunan Province, Scientific research project of Xiangnan University ([2022]96),

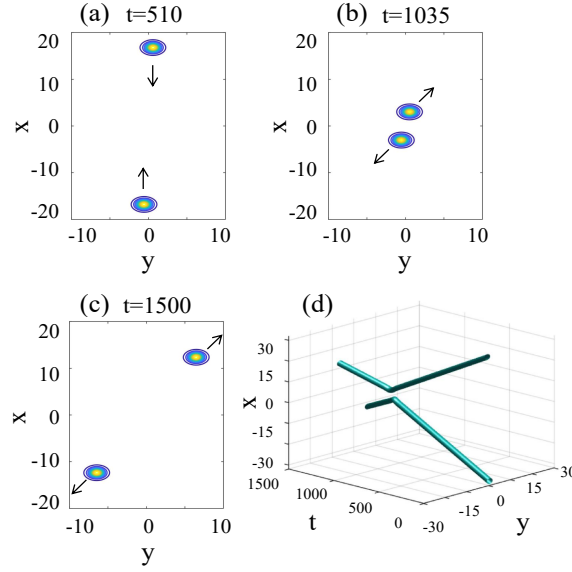


FIG. 10. Collisions between SV solitons moving with opposite velocities, $V_x = \pm 0.03$. Contour and isosurface plots of $|\Psi_+|^2 + |\Psi_-|^2$ are displayed at $t = 510$ (a), $t = 1035$ (b), $t = 1500$ (c), and (d) (isosurface plot). Here, parameters of the SV solitons are selected as $(N, g_{\pm}, \gamma, S_+) = (4, 1, 1, 0)$.

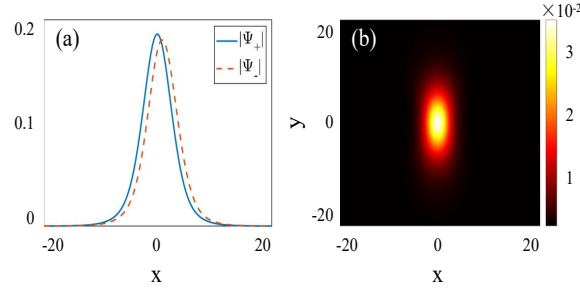


FIG. 11. An example of a stable mixed mode with parameters $(N, g_{\pm}, \gamma, V_x, V_y) = (4, 1, 1, 0, 0.1)$. (a) One-dimensional cross sections of the two components, $|\Psi_+|$ and $|\Psi_-|$. Panel (b) displays the density patterns of vortex component, $|\Psi_+|^2$.

and Israel Science Foundation (grant No. 1695/22).

-
- [1] M. H. Anderson, J. R. Ensher, M. R. Matthews, C. E. Wieman, and E. A. Cornell, Observation of Bose-Einstein condensation in a dilute atomic vapor, *Science* 269, 198 (1995).
 - [2] C. C. Bradley, C. A. Sackett, J. J. Tollett, and R. G. Hulet, Evidence of Bose-Einstein condensation in an atomic gas with attractive interactions, *Phys. Rev. Lett.* 75, 1687 (1995).
 - [3] K. B. Davis, M. O. Mewes, M. R. Andrews, N. J. van Druten, D. S. Durfee, D. M. Kurn, and W. Ketterle, Bose-Einstein condensation in a gas of sodium atoms, *Phys. Rev. Lett.* 75, 3969 (1995).
 - [4] J. E. Williams, and M. J. Holl, Preparing topological states of a Bose-Einstein condensate, *Nature* 401, 568 (1999).
 - [5] K. Kasamatsu, M. Tsubota, and M. Ueda, Vortex phase diagram in rotating two-component Bose-Einstein condensates, *Phys. Rev. Lett.* 91, 150406 (2003).
 - [6] S. Burger, S. Bongs, S. Dettmer, W. Ertmer, and K. Sengstock, Dark solitons in Bose-Einstein condensates, *Phys. Rev. Lett.* 83, 5198 (1999).
 - [7] B. P. Anderson, P. C. Haljan, C. A. Regal, D. L. Feder, L. A. Collins, C. W. Clark, and E. A. Cornell, Watching dark solitons decay into vortex rings in a Bose-Einstein condensate, *Phys. Rev. Lett.* 86, 2926 (2001).
 - [8] K. E. Strecker, G. B. Partridge, A. G. Truscott, and R. G. Hulet, Formation and propagation of matter-wave soliton trains, *Nature* 417, 150-153 (2002).
 - [9] L. Khaykovich, F. Schreck, G. Ferrari, T. Bourdel, J. Cubizolles, L. D. Carr, Y. Castin, and C. Salomon, Formation of a matter-wave bright soliton", *Science* 296, 1290-1293 (2002).

- [10] B. Eiermann, Th. Anker, M. Albiez, M. Taglieber, P. Treutlein, K.-P. Marzlin, and M. K. Oberthaler, Bright Bose-Einstein gap solitons of atoms with repulsive interaction, *Phys. Rev. Lett.* 92, 230401 (2004).
- [11] C.-A. Chen and C.-L. Hung, Observation of universal quench dynamics and Townes soliton formation from modulational instability in two-dimensional Bose gases, *Phys. Rev. Lett.* 125, 250401 (2020).
- [12] B. Bakkali-Hassani, C. Maury, Y.-Q. Zhou, E. Le Cerf, R. Saint-Jalm, P. C. M. Castilho, S. Nascimbene, J. Dalibard, and J. Beugnon, Realization of a Townes soliton in a two-component planar Bose gas, *Phys. Rev. Lett.* 127, 023603 (2021).
- [13] C. Cabrera, L. Tanzi, J. Sanz, B. Naylor, P. Thomas, P. Cheiney, and L. Tarruell, Quantum liquid droplets in a mixture of Bose-Einstein condensates, *Science* 359, 301-304 (2018).
- [14] P. Cheiney, C. R. Cabrera, J. Sanz, B. Naylor, L. Tanzi, and L. Tarruell, Bright soliton to quantum droplet transition in a mixture of Bose-Einstein condensates, *Phys. Rev. Lett.* 120, 135301 (2018).
- [15] G. Semeghini, G. Ferioli, L. Masi, C. Mazzinghi, L. Wolswijk, F. Minardi, M. Modugno, G. Modugno, M. Inguscio, and M. Fattori, Self-bound quantum droplets of atomic mixtures in free space?, *Phys. Rev. Lett.* 120, 235301 (2018).
- [16] M. Albiez, R. Gati, J. Fölling, S. Hunsmann, M. Cristiani, and M. K. Oberthaler, Direct observation of tunneling and nonlinear self-trapping in a single bosonic Josephson junction, *Phys. Rev. Lett.* 95, 010402 (2005).
- [17] W. C. Syu, D. S. Lee, and C. Y. Lin, Regular and chaotic behavior of collective atomic motion in two-component Bose-Einstein condensates, *Phys. Rev. A* 101, 063622 (2020).
- [18] C. Lee, W. Hai, L. Shi, X. Zhu, and K. Gao, Chaotic and frequency-locked atomic population oscillations between two coupled Bose-Einstein condensates, *Phys. Rev. A* 64, 053604 (2001).
- [19] H. Edri, B. Raz, G. Fleurov, R. Ozeri, and N. Davidson, Observation of nonlinear spin dynamics and squeezing in a BEC using dynamic decoupling, *New J. Phys.* 23, 053005 (2021).
- [20] C. Kong, H. Chen, C. Li, W. Hai, Controlling chaotic spin-motion entanglement of ultracold atoms via spin-orbit coupling, *Chaos* 28, 023115(2018); C. Kong, Y. He, T. Wan, B. Yin, R. Liu, Y. Chen, J. Huang, D. Lei, C. Jiang, and H. Deng, Excitation of chaotic atomic population oscillations in a spin-orbit coupled Bose-Einstein condensate with a square-wave driving, *Phys. Lett. A* 458, 128597 (2023).
- [21] R. Y. Chiao, E. Garmire, and C. H. Townes, Self-trapping of optical beams, *Phys. Rev. Lett.* 13, 479-482 (1964).
- [22] L. Bergé, Wave collapse in physics: Principles and applications to light and plasma waves, *Phys. Rep.* 303, 259 (1998).
- [23] C. Sulem, and P. L. Sulem, *Nonlinear Schrödinger equations: self-focusing instability and wave collapse*, New York: Science Business Media; 2007.
- [24] G. Fibich, *The nonlinear Schrödinger equation: singular solutions and optical collapse*, Berlin: Heidelberg; 2015.
- [25] B. A. Malomed, D. Mihalache, F. Wise, and L. Torner, Spatiotemporal optical solitons, *J. Opt. B* 7, R53 (2005).
- [26] B. A. Malomed, *Multidimensional Solitons* (AIP Publishing, Melville, NY, 2022).
- [27] D. S. Petrov, Quantum mechanical stabilization of a collapsing Bose-Bose mixture, *Phys. Rev. Lett.* 115, 155302 (2015).
- [28] D. S. Petrov and G. E. Astrakharchik, Ultradilute low-dimensional liquids, *Phys. Rev. Lett.* 117, 100401 (2016).
- [29] Z. Luo, W. Pang, B. Liu, Y. Li, and B. A. Malomed, A new form of liquid matter: Quantum droplets, *Front. Phys.* 16, 32201 (2021).
- [30] P. Pedri, and L. Santos, Two-Dimensional Bright Solitons in Dipolar Bose-Einstein Condensates, *Phys. Rev. Lett.* 95, 200404 (2005).
- [31] R. Nath, P. Pedri, and L. Santos, Stability of Dark Solitons in Three-Dimensional Dipolar Bose-Einstein Condensates, *Phys. Rev. Lett.* 101, 210402 (2008).
- [32] I. Tikhonenkov, B. A. Malomed, and A. Vardi, Anisotropic Solitons in Dipolar Bose-Einstein Condensates, *Phys. Rev. Lett.* 100, 090406 (2008).
- [33] M. Raghunandan, C. Mishra, K. Lakomy, P. Pedri, L. Santos, and R. Nath, Two-dimensional bright solitons in dipolar Bose Einstein condensates with tilted dipoles, *Phys. Rev. A* 92, 013637 (2015).
- [34] J. Huang, X. Jiang, H. Chen, Z. Fan, W. Pang, and Y. Li, Quadrupolar matter-wave soliton in two-dimensional free space, *Front. Phys.* 10, 100507 (2015).
- [35] H. Sakaguchi, B. Li, and B. A. Malomed, Creation of two-dimensional composite solitons in spin-orbit-coupled self-attractive Bose-Einstein condensates in free space, *Phys. Rev. E* 89, 032920 (2014).
- [36] X. Jiang, Z. Fan, Z. Chen, W. Pang, Y. Li, and B. A. Malomed, Two-dimensional solitons in dipolar Bose-Einstein condensates with spin-orbit coupling, *Phys. Rev. A* 93, 023633(2016).
- [37] B. Liao, S. Li, C. Huang, Z. Luo, W. Pang, H. Tan, B. A. Malomed, and Y. Li, Anisotropic semivortices in dipolar spinor condensates controlled by Zeeman splitting, *Phys. Rev. A* 96, 043613 (2017).
- [38] S. Gautam and S. K. Adhikari, Vortex-bright solitons in a spin-orbit-coupled spin-1 condensate, *Phys. Rev. A* 95, 013608 (2017).
- [39] G. Chen, Y. Liu, and H. Wang, Mixed-mode solitons in quadrupolar BECs with spin-orbit coupling, *Commun. Nonlinear Sci. Numer. Simul.* 48, 318 (2017).
- [40] Y. Zhang, Z. Zhou, B. A. Malomed, and H. Pu, Stable solitons in three dimensional free space without the ground state: Self-trapped Bose-Einstein condensates with spin-orbit coupling, *Phys. Rev. Lett.* 115 253902 (2015).
- [41] Y. Zhang, M. E. Mossman, T. Busch, P. Engels, and C. Zhang, Properties of spin-orbit-coupled Bose-Einstein condensates, *Front. Phys.* 11, 118103 (2016).
- [42] Y. Li, X. Zhang, R. Zhong, Z. Luo, B. Liu, C. Huang, W. Pang, and B. A. Malomed, Two-dimensional composite solitons in Bose-Einstein condensates with spatially confined spin-orbit coupling, *Commun. Nonlinear Sci. Numer. Simul.* 73, 481 (2019).
- [43] X. Chen, Z. Deng, X. Xu, S. Li, Z. Fan, Z. Chen, B. Liu, and Y. Li, Nonlinear modes in spatially confined spin-orbit-coupled Bose-Einstein condensates with repulsive nonlinearity, *Nonlinear. Dyn.* 101, 569 (2020).

- [44] G. Roati, M. Zaccanti, C. D'Errico, J. Catani, M. Modugno, A. Simoni, M. Inguscio, and G. Modugno, ^{39}K Bose-Einstein condensate with tunable interactions, *Phys. Rev. Lett.* 99, 010403 (2007).
- [45] S. B. Papp, J. M. Pino and C. E. Wieman, Tunable miscibility in a dual-species Bose-Einstein condensate, *Phys. Rev. Lett.* 101, 040402 (2008).
- [46] P. Zhang, P. Naidon and M. Ueda, Independent control of scattering lengths in multicomponent quantum gases, *Phys. Rev. Lett.* 103 133202 (2009).
- [47] C. Chin, R. Grimm, P. Julienne, and E. Tiesinga, Feshbach resonances in ultracold gases, *Rev. Mod. Phys.* 82, 1225-1286 (2010).
- [48] M. Vakhitov, and A. Kolokolov, Stationary solutions of the wave equation in the medium with nonlinearity saturation, *Radiophys. Quantum Electron.* 16, 783 (1973).
- [49] H. Sakaguchi and B. A. Malomed. Solitons in combined linear and nonlinear lattice potentials, *Phys. Rev. A* 81, 013624 (2010).
- [50] C. Huang, Y. Ye, S. Liu, H. He, W. Pang, B. A. Malomed, and Y. Li, Excited states of two-dimensional solitons supported by spin-orbit coupling and field-induced dipole-dipole repulsion, *Phys. Rev. A* 97, 013636 (2018).
- [51] R. Zhong, Z. Chen, C. Huang, Z. Luo, H. Tan, B. A. Malomed, Y. Li, Self-trapping under two-dimensional spin-orbit coupling and spatially growing repulsive nonlinearity, *Front. Phys.* 13, 130311 (2018).
- [52] W. J. Thompson, *Angular Momentum: An Illustrated Guide to Rotational Symmetries for Physical Systems*, Volume 1 (Wiley-VCH, Hoboken, New Jersey, 1994).
- [53] W. Z. Bao and Q. Du, Computing the ground state solution of Bose-Einstein condensates by a normalized gradient flow, *SIAM J. Sci. Comp.* **25**, 1674-1697 (2004).
- [54] Z. Chen, Y. Li, and B. A. Malomed, Josephson oscillations of chirality and identity in two-dimensional solitons in spin-orbit-coupled condensates, *Phys. Rev. Research* 2, 033214 (2020).
- [55] H. Kadau, M. Schmitt, M. Wenzel, C. Wink, T. Maier, I. Ferrier-Barbut, and T. Pfau, Observing the Rosensweig instability of a quantum ferrofluid, *Nature* 530,194 (2016).
- [56] I. Ferrier-Barbut, H. Kadau, M. Schmitt, M. Wenzel, and T. Pfau, Observation of quantum droplets in a strongly dipolar Bose gas, *Phys. Rev. Lett.* 116, 215301 (2016).
- [57] B. A. Malomed, The family of quantum droplets keeps expanding, *Front. Phys.* 16, 22504 (2021).
- [58] X. Zhang, X. Xu, Y. Zheng, Z. Chen, B. Liu, C. Huang, B. A. Malomed, and Y. Li, Semidiscrete quantum droplets and vortices, *Phys. Rev. Lett.* 123, 133901 (2019).
- [59] Y. Li, Z. Luo, Y. Liu, Z. Chen, C. Huang, S. Fu, H. Tan, and B. A. Malomed, Two-dimensional solitons and quantum droplets supported by competing self-and cross-interactions in spin-orbit-coupled condensates, *New J. Phys.* 19, 113043 (2017).
- [60] G. Li, X. Jiang, B. Liu, Z. Chen, B. A. Malomed, and Y. Li, Two-dimensional anisotropic vortex quantum droplets in dipolar Bose-Einstein condensates, *Front. Phys.* 19, 22202 (2024).
- [61] Y. Li, Z. Chen, Z. Luo, C. Huang, H. Tan, W. Pang, and B. A. Malomed, Two-dimensional vortex quantum droplets, *Phys. Rev. A* 98, 063602 (2018).